Available online at www.sciencedirect.com
ScienceDirect
Journal of Computational Physics 222 (2007) 536–555
JOURNAL OF COMPUTATIONAL PHYSICS
www.elsevier.com/locate/jcp

A level set based sharp interface method for the multiphase incompressible Navier–Stokes equations with phase change

Frédéric Gibou [a,*], Liguo Chen [b], Duc Nguyen [c], Sanjoy Banerjee [d]

[a] *Mechanical Engineering Department and Computer Science Department, University of California, Santa Barbara, CA 93106, United States*
[b] *Mechanical Engineering Department, University of California, Santa Barbara, CA 93106, United States*
[c] *Lockheed Martin Missiles & Space, 1111 Lockheed Martin Way Sunnyvale, CA 94089, United States*
[d] *Mechanical Engineering Department & Chemical Engineering Department, University of California, Santa Barbara, CA 93106, United States*

Received 23 November 2005; received in revised form 8 May 2006; accepted 29 July 2006
Available online 17 October 2006

Abstract

In this paper, we describe a sharp interface capturing method for the study of incompressible multiphase flows with phase change. We use the level set method to keep track of the interface between the two phases and a ghost fluid approach to impose the jump conditions at the interface. This work builds on the work of Gibou et al. for the study of Stefan problems [F. Gibou, R. Fedkiw, L.-T. Cheng, M. Kang, A second-order-accurate symmetric discretization of the Poisson equation on irregular domains, J. Comput. Phys. 176 (2002) 205–227] and the work of Nguyen et al. for the simulation of incompressible flames [D. Nguyen, R. Fedkiw, M. Kang, A boundary condition capturing method for incompressible flame discontinuities, J. Comput. Phys. 172 (2001) 71–98]. We compare our numerical results to exact solutions in one spatial dimension and apply this algorithm to the simulation of film boiling in two spatial dimensions.

1. Introduction

Over the last two decades, there has been on ongoing quest for new computational methods to solve multiphase flows with phase change. This thrust has been motivated in part by the energy industry because phase change processes allow fluids to store and release large amounts of heat energy. Other applications include the study of condensation in the context of manned space flight dehumidification and thermal management

* Corresponding author.
E-mail address: fgibou@engineering.ucsb.edu (F. Gibou).

0021-9991/$ - see front matter © 2006 Elsevier Inc. All rights reserved.
doi:10.1016/j.jcp.2006.07.035

systems, particularly difficult to study experimentally in microgravity environments and of considerable interest to NASA.

Numerical simulations offer a promising avenue and several approaches have been introduced in the last two decades. The main challenges for a direct numerical simulation come from the fact that the interface location must be calculated as part of the solution process and because discontinuities in materials properties across the interface must be preserved. Finally, the problem involves dissimilar length scales with smaller scales influencing larger ones so that non-trivial pattern formation dynamics can be expected to occur on all intermediate scales. This results in a highly nonlinear problem that is very sensitive to numerical errors and prone to numerical instabilities.

The first attempt at advanced numerical simulations can be attributed to Welch who presented the simulation of a two-dimensional thin film boiling using moving triangular grids [32]. In this case, the difficulty associated with grid topology as it deformed limited the simulation to short times. Similar limitations were encountered in the moving body fitted approach of Son and Dhir [29]. Juric and Tryggvason presented a front tracking approach to the simulation of boiling flows in [18]. Their approach is based on the so-called single field formulation where only one set of equations describes the entire flow field and relies on a delta function formulation to impose interfacial source terms. Also, the phase boundary is tracked explicitly by a moving front on a fixed Cartesian grid. This approach has produced remarkable results but topological changes like merging and pinching are not straightforward to handle, especially in three spatial dimensions. Similar simulations were carried out by Son and Dhir [30] using a level set approach as well as Tomar et al. using a coupled level set and volume of fluid approach [34]. The advantage of the level set method is that topological changes are handled naturally without special treatments. However, the authors used a delta function formulation as in [31] to represent the discontinuities across the phase interface, leading to a smeared out profile of the different variables. Welch and Wilson introduced a volume-of-fluid approach using similar smearing of the discontinuous variables [33].

In this paper, we draw on the work of Gibou et al. [12] and Nguyen et al. [22] to propose a sharp interface capturing method for the direct numerical simulation of multiphase incompressible flows with phase change. In particular, we use a level set approach to capture the evolution of the interface location and the ghost fluid method for imposing the jump conditions at the interface. We emphasize that our treatment preserves the discontinuous nature of all the variables across the phase interface except for the viscosity, for which we use a delta formulation mechanism for simplicity. The smearing of the viscosity across the interface significantly ease the formulation (see [19]). In fact, the sharp treatment of the viscosity presented in [19] does not apply to the case of phase change. We compare our numerical results on one-dimensional test problems and apply our algorithm to the simulation of two-dimensional thin boiling films.

2. Equations

Consider a domain $\Omega \in \mathbb{R}^n$ and a lower dimensional interface Γ that divides Ω into disjoint subdomains Ω^- and Ω^+. We describe the behavior of each phase in Ω^- and Ω^+ by the incompressible Navier–Stokes equations, and account for interfacial phase change by deriving the jump conditions that must be satisfied at the interface.

2.1. The incompressible Navier–Stokes equations

The basic equations for viscous incompressible flows that describe the conservation of momentum and mass read

$$\rho(\vec{V}_t + (\vec{V}\cdot\nabla)\vec{V}) = -\nabla P + \rho\vec{g} + \nabla\cdot[\mu(\nabla\vec{V} + (\nabla\vec{V})^{\mathrm{T}})], \tag{1}$$

$$\nabla\cdot\vec{V} = 0, \tag{2}$$

where t is the time, ρ the density, $\vec{V} = \langle u, v\rangle$ the velocity field, p the pressure, μ the viscosity and $\vec{g} = \langle 0, -g\rangle$ the gravity field.

2.2. Conservation of energy

The conservation of internal energy per unit mass e yields

$$\rho e_t + \rho \vec{V} \cdot \nabla e = \nabla \cdot \vec{q} + \tau : \nabla \vec{V} - P \nabla \cdot \vec{V}, \tag{3}$$

where $\vec{q}$ is the heat flux, $-P\nabla \cdot \vec{V}$ is the pressure work and where $\tau : \nabla \vec{V}$ represents the viscous dissipation. Often, the viscous dissipation can be considered small compared to the heat flux. Assuming e depends on at most temperature, and that the specific heat at constant volume, c_v, is constant leads to $e = e_0 + c_v(T - T_0)$, where e_0 is the internal energy per unit mass at some reference temperature T_0 [2]. Also, we assume that the constitutive relation for the heat flux, $\vec{q} = -k\nabla T$, holds throughout the entire domain. Using the incompressibility condition, $\nabla \cdot \vec{V} = 0$, we can neglect the pressure work. Furthermore, neglecting the viscous dissipation we can simplify Eq. (3) to

$$\rho c_v T_t + \rho c_v \vec{V} \cdot \nabla T = \nabla \cdot (k \nabla T).$$

Finally, if k is a constant on some domain, we can obtain the simpler advection–diffusion equation for the temperature

$$T_t + \vec{V} \cdot \nabla T = \alpha \nabla^2 T, \tag{4}$$

where $\alpha = k/\rho c_v$ is the thermal diffusivity.

2.3. Interface velocity and jump conditions

Liquid and *Vapor* phases are separated by an interface across which the phase change occurs (i.e. liquid vaporizes into vapor or vapor condenses onto liquid). We use the subscripts "l" and "v" to refer to the liquid and vapor phases, respectively. The interface velocity is denoted by $\vec{W} = D\vec{N}$, where D is the normal component of the interface velocity and $\vec{N} = \langle n_1, n_2 \rangle$ is the local unit outward normal to the interface. If we let M be the interfacial mass flux, we get from the conservation of mass across the interface:

$$M = \rho_l((V_N)_l - D) = \rho_v((V_N)_v - D), \tag{5}$$

where $V_N = \vec{V} \cdot \vec{N}$ is the normal velocity. The temperature at the interface is assumed to satisfy (see [16])

$$T_l = T_v = T_{sat}, \tag{6}$$

where $T_{sat} = T(P_{interface})$ is the saturation temperature, as pressure fluctuations are small compared to the absolute pressure. Integration of Eq. (4) across the interface along with Eq. (6) gives the following Rankine–Hugoniot jump condition for the energy conservation (neglecting the small kinetic energy contributions)

$$[\rho h(V_N - D)] = [-k\nabla T \cdot \vec{N}], \tag{7}$$

where $[A] = A_v - A_l$ defines the jump in the quantity A across the interface and h defines the enthalpy. We assume that h depends only on temperature, and that the specific heat at constant pressure $c_p = c_v$. Eqs. (5) and (7) give

$$M = [-k\nabla T \cdot \vec{N}]/[H], \tag{8}$$

where $[H] = h_v - h_l$ is the latent heat of phase change. We can then calculate the interface velocity D and the velocity jump across the interface as

$$D = (V_N)_l + M/\rho_l = (V_N)_v + M/\rho_v, \tag{9}$$

$$[V_N] = M\left[\frac{1}{\rho}\right]. \tag{10}$$

As pointed out in [22], it is more natural to write

$$[\vec{V}] = M\left[\frac{1}{\rho}\right]\vec{N} \tag{11}$$

to emphasize that the jump in the normal component of the velocity is given by Eq. (10) and that the jump in the tangential component is zero. Finally, integrating Eq. (1) across the interface and including the effects of surface tension leads:

$$\left[P - \mu\frac{\partial V_N}{\partial N} + \rho(V_N - D)^2\right] = \sigma\kappa, \tag{12}$$

which gives the jump in pressure

$$[P] = \sigma\kappa - [\rho(V_N - D)^2] + \left[\mu\frac{\partial V_N}{\partial N}\right]. \tag{13}$$

2.4. The level set method

The level set method was introduced by Osher and Sethian [24] as a general technique to keep track of a moving interface in a capturing framework. The main advantage of this method is its ability to handle topological changes in a straightforward fashion. On coarse grids, the loss of mass inherent to the original level set approach was overcome by Enright et al. [8] in the case of externally generated velocities, which is the case for incompressible flows. We note that although we do not use this technique in this paper, mainly because we consider grids fine enough, the addition of particles would be straightforward.

In this work, the level set function ϕ is used to separate the liquid and the vapor phases as the set of points where $\phi < 0$ and $\phi > 0$, respectively. The interface is designated by the set of points where $\phi = 0$. The motion of the interface with velocity $\vec{W}$ is captured by evolving the level set equation

$$\phi_t + \vec{W}\cdot\nabla\phi = 0. \tag{14}$$

In order to produce robust numerical results, it is desirable to keep the values of ϕ close to those of a signed distance function, i.e. $|\nabla\phi| = 1$. This is achieved by iterating the so-called reinitialization equation [31]

$$\phi_\tau + S(\phi_0)(|\nabla\phi| - 1) = 0, \tag{15}$$

for a few steps in fictitious time τ. Here $S(\phi_0) = \phi_0/\sqrt{\phi_0^2 + \epsilon}$ is a smoothed out sign function, with $\epsilon = \max(\Delta x, \Delta y)^2$. The Hamilton–Jacobi equations (14) and (15) are solved with a fifth-order HJ-WENO scheme [17]. The level set function is used to compute the normal to the interface $\vec{N} = \nabla\phi/|\nabla\phi|$ and the interface mean curvature $\kappa = -\nabla\cdot\vec{N}$ using standard central differencing. The interested reader is referred to the book by Osher and Fedkiw [23] and the book by Sethian [27] for more details on the level set method.

3. Numerical method

The spatial discretization of the governing equations is obtained using a traditional MAC staggered grid [15] (see also [25]) with the scalars located at the cell centers ($\rho_{i,j}$, $P_{i,j}$, $\phi_{i,j}$, $T_{i,j}$) and the velocity components located at the appropriate cell edges ($u_{i+1/2,j}$, $v_{i,j+1/2}$). We adopt a standard projection method [6] (see also [4,14]) for solving the incompressible Navier–Stokes equations and an implicit Crank–Nicholson scheme for solving the heat equation.

3.1. The projection method

The projection method for one-phase incompressible flows consists of three stages: first, given the velocity field at time t^n, an intermediate velocity $\vec{V}^*$ is calculated by ignoring the pressure component

$$\frac{\vec{V}^* - \vec{V}^n}{\Delta t} + \vec{V}^n\cdot\nabla\vec{V}^n = \vec{g} + \frac{1}{\rho^n}\nabla\cdot[\mu(\nabla\vec{V}^n + (\nabla\vec{V}^n)^{PT})]. \tag{16}$$

In order for the velocity $\vec{V}^{n+1}$ to satisfy the incompressibility condition $\nabla\cdot\vec{V}^{n+1} = 0$ the second stage defines the pressure p^{n+1} through the solution of the Poisson equation

$$\nabla \cdot \left(\frac{\nabla p^{n+1}}{\rho^{n+1}} \right) = \frac{\nabla \cdot \vec{V}^*}{\Delta t}. \tag{17}$$

In the last stage the fluid velocity $\vec{V}^{n+1}$ at the new time step t^{n+1} is projected onto the divergence free field

$$\vec{V}^{n+1} = \vec{V}^* - \Delta t \frac{\nabla p^{n+1}}{\rho^{n+1}}. \tag{18}$$

In Eq. (16), the convection term is discretized using high order upwind methods, e.g. third-order accurate ENO [28] and fourth-order accurate WENO [20] schemes. The discretization of the viscosity term is performed using standard central differencing formulae. Treating the viscosity implicitly is desirable since the time step restriction associated with the parabolic equation can be stringent. However, it is not clear how to treat the viscosity implicitly in the case of two-phase flows with phase change. We note that the coefficient controlling the amount of viscosity is expected to be small in this work and therefore an explicit treatment of the viscosity is appropriate.

3.2. Solving the energy equation

In the case of one-phase flows, i.e. without an interface, the Crank–Nicholson scheme for the heat equation,

$$\frac{T^{n+1} - T^n}{\Delta t} = \frac{1}{2} \nabla \cdot (k \nabla T^{n+1}) + \frac{1}{2} \nabla \cdot (k \nabla T^n)$$

yields second-order accuracy in both space and time with a time step of $\Delta t \approx \Delta x$. Each equation is used to fill one row of a linear system for the unknowns $T_{i,j}^{n+1}$, which can be solved using fast solvers (e.g. the conjugate gradient using an Incomplete Cholesky preconditioner [PCG] [13,26]). In this work we also need to account for the advection of the temperature, i.e. $\vec{V} \cdot \nabla T$, which is discretized explicitly at time level t^n. The scheme used for solving the energy equation is then given by

$$\frac{T^{n+1} - T^n}{\Delta t} = \frac{1}{2} \nabla \cdot (k \nabla T^{n+1}) + \frac{1}{2} \nabla \cdot (k \nabla T^n) - \vec{V}^n \cdot \nabla T^n, \tag{19}$$

where the convection term is discretized using a fourth-order WENO method [20].

3.3. Imposing the interface boundary conditions

Special care needs to be taken when discretizing equations (16)–(19) in the case of a moving interface across which jump conditions must be satisfied. This stems from the fact that as the interface is evolved form t^n to t^{n+1}, i.e. ϕ^n is evolved to ϕ^{n+1}, the interface sweeps some grid points that do not yet hold valid values for the quantities to be discretized. In [10], Fedkiw et al. introduced the Ghost Fluid Method to treat contact discontinuities in the case of multiphase compressible flows with no phase change. This philosophy was then applied to a wide range of applications (see [5,9,12,19,21,22] and the references therein). In this paper, we combine the work of Gibou et al. for the Stefan problem [12] and the work of Nguyen et al. for incompressible flame [22] to propose a sharp interface approach to incompressible flows with phase change.

3.3.1. Interface boundary conditions for the temperature

The interface boundary condition for the temperature is treated in a similar fashion as in [12]. First consider the Poisson equation $T_{xx} = f$ in one spatial dimension in a domain Ω separated in two regions Ω^- and Ω^+. Suppose that the interface x_I lies in between two grid points x_i and x_{i+1}. Standard second-order accurate central differencing formulae can be applied to all the grid nodes inside the domain, except for those adjacent to the interface. In this case, special care needs to be taken in order to discretize T_{xx} using only values from the same side of the interface. For example, consider the situation depicted in Fig. 1 and the standard discretization at x_i

$$\frac{T_{i-1} - 2T_i + T_{i+1}}{\Delta x}. \tag{20}$$

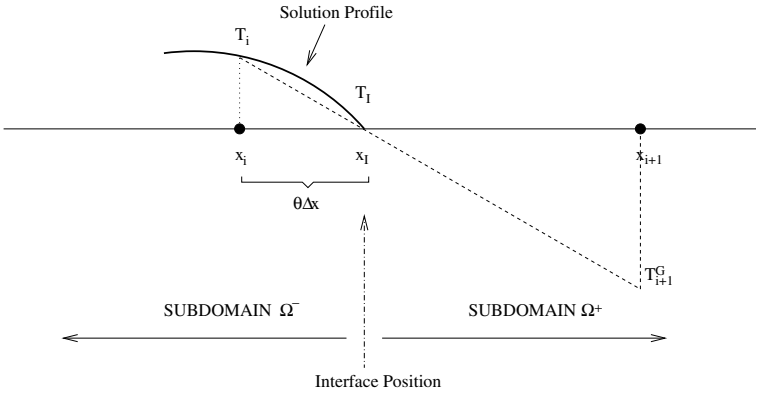

Fig. 1. Definition of the ghost cells with linear extrapolation. First, we construct a linear interpolant $\widetilde{T}(x) = ax + b$ of T such that $\widetilde{T}(0) = T_i$ and $\widetilde{T}(\theta\Delta x) = T_I$. Then we define $T^{\mathrm{G}}_{i+1} = \widetilde{T}(\Delta x)$.

To avoid differencing across the interface (to avoid the jump in ∇T), we use a ghost value for T_{i+1}, defined by extrapolating the data to the left of x_I. In [12], Gibou et al. showed that a linear extrapolation is sufficient to produce second-order accurate solutions while conserving the symmetry in the linear system. In turn, this system can be inverted quickly using fast solvers like PCG [13,26]. Likewise, the discretization at x_{i+1} involves constructing an interpolant using values to the right of x_I only. Numerical schemes using higher order extrapolations have also been presented in Gibou and Fedkiw [11].

This approach can be applied in a dimension by dimension framework and is trivially extended to the solution of the heat equation. For example consider the case of the Crank–Nicholson scheme

$$\left(I - \frac{\Delta t}{2}\Delta^{n+1}\right)T^{n+1} = \left(I - \frac{\Delta t}{2}\Delta^{n}\right)T^{n}, \tag{21}$$

where I is the identity matrix and Δ^n and Δ^{n+1} are the discretizations of the Laplacian at time t^n and t^{n+1}, respectively. We first discretize the right-hand side of this equation, using ghost values for grid nodes adjacent to the interface as described above. Then, a linear system of equations is constructed by discretizing the left-hand side in a similar way as for the Poisson equation discussed above. In the case of a moving interface, we need to account for the fact that grid points are swept over by the interface and might not hold valid value of the solution T^n as depicted in Fig. 2. In this case, ghost values are defined by linear extrapolation in the normal

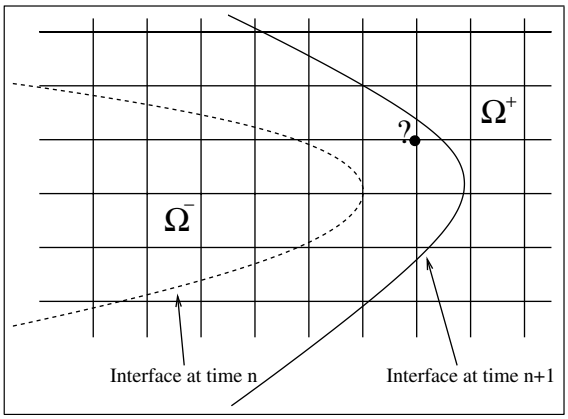

Fig. 2. Interface at two consecutive time steps t^n (dashed line) and t^{n+1} (solid line). The dark point with a question mark represents a grid node that is swept over by the interface between the two consecutive time steps and where a valid value of T^n needs to be extrapolated in a non-Cartesian normal direction in order to evaluate $(I - \frac{\Delta t}{2}\Delta^n)T^n$ in Eq. (21).

direction. This extrapolation can be performed as described in [12], but we also mention that a general way to extrapolate in the normal direction to high order accuracy is described in [1].

3.3.2. Interface boundary conditions for the velocity

Eq. (8) is used to find the phase change mass rate M using the jump in temperature gradients $[k\nabla T \cdot \vec{N}]$ across the interface. The evaluation of this term requires the computation of T_x and T_y at the interface in each subdomains Ω^- and Ω^+. For example referring to Fig. 1, we compute T_x^- at x_i by simply differentiating the interpolation polynomial $\widetilde{T}$, hence avoiding differentiating across the interface. We note that this discretization is prone to numerical errors in the case where the interface is very close to the interface. In this case, the value of T at x_I and x_{i-1} are used in the construction of the interpolant $\widetilde{T}$ instead of the value of T at x_I and x_{i-1} (see [12] for more details). The value of T_x^- at x_i is then extrapolated across the interface in a constant fashion, defining ghost values for T_x^- in Ω^+. Likewise the value of T_x^+ at x_{i+1} is computed using an interpolant constructed with value of T in Ω^+ only and is then extrapolated across the interface to define ghost values of T_x^+ in Ω^-. T_y is treated similarly. The jump in $[k\nabla T \cdot \vec{N}]$ is then calculated at each nodes in a band around the interface using the real and the ghost values of the derivatives T_x and T_y.

Once M is computed, Eqs. (9) and (10) are used to find the interface velocity and the velocity's jump. In order to avoid the difficulty that arises when nodal values change character (i.e. from liquid to vapor or vice-versa) as the interface moves, we follow the methodology introduced in Nguyen et al. [22] and define a band of ghost velocities on both sides of the interface: for example, at every locations where the velocity of the vapor phase is defined, the jump condition given by (10) is used to define a ghost velocity for the liquid phase

$$u_l^G = u_v - M\left(\frac{1}{\rho_v} - \frac{1}{\rho_l}\right)n_1, \tag{22}$$

$$v_l^G = v_v - M\left(\frac{1}{\rho_v} - \frac{1}{\rho_l}\right)n_2, \tag{23}$$

where n_1 and n_2 are computed at the appropriate MAC grid locations using simple averaging. Similarly, vapor ghost velocities are calculated at the MAC grid locations occupied by the liquid phase.

It is important to note that the ghost values of the extended velocity field are used in the discretization of $\vec{V}^*$. That is, liquid fluid velocities are discretized with the aid of the liquid ghost velocities avoiding the use of any vapor velocities that would pollute the solution. Likewise, the vapor fluid velocities are discretized using their ghost values avoiding the liquid fluid velocities in the discretization. And values for $\vec{V}^*$ are determined on the appropriate side of the interface and on a band including the interface. This is done to alleviate problems that occur when the interface moves through the grid changing character of the solution from liquid to vapor or vice-versa.

Finally, we note that in the case where one needs to impose a Dirichlet boundary condition for $\vec{V}^{n+1}$, one simply applies this condition to $\vec{V}^*$, then sets $\nabla p \cdot \vec{N} = 0$ on the domain boundary.

The level set function is evolved in time from ϕ^n to ϕ^{n+1} using the nodal velocities, $\vec{W} = D\vec{N}$. The nodal values of the liquid velocity, $\vec{v}_l$ are determined using simple averaging of the MAC grid values using use the appropriate ghost values (defined above) where needed. Then $(V_N)_l = \vec{V}_l \cdot \vec{N}$ is used to define the liquid normal velocity at each grid node.

3.3.3. Interface boundary conditions for the pressure

Once $\vec{V}^*$ has been updated, we solve the Poisson equation for the pressure given by Eq. (17) with the jump condition given by Eq. (13): first, we compute the divergence of V^* in Eq. (17) using standard central differencing

$$(u_x^*)_{i,j} = \frac{u^*_{i+1/2,j} - u^*_{i-1/2,j}}{\Delta x}, \tag{24}$$

$$(u_y^*)_{i,j} = \frac{u^*_{i,j+1/2} - u^*_{i,j-1/2}}{\Delta y}, \tag{25}$$

then we use the method proposed in Liu et al. [21] to build the linear system associated with the discretization of $\nabla \cdot \left(\frac{\nabla p^{n+1}}{\rho^{n+1}}\right)$ using the jump condition given by Eq. (13). In [19], Kang et al. pointed out that one can set $\left[\frac{p_x}{\rho}\right] = \left[\frac{p_y}{\rho}\right] = 0$ at the domain's boundary when solving the Poisson equation, even though the jump conditions for $\left[\frac{p_x}{\rho}\right]$ and $\left[\frac{p_y}{\rho}\right]$ are non-zero. This is because the jumps in the pressure derivatives in Eq. (17) are balanced through the definition of V^* and because Eq. (1) is continuous across the interface, allowing one to take the divergence of the entire equation without considering the jumps.

We emphasize that this discretization preserve the discontinuous character of the solution and that the linear system is symmetric, allowing for fast solvers to be used, i.e. we use the preconditioned conjugate gradient method (see [13,26]).

3.3.4. Treatment of the viscous term

In this work, the viscosity is treated using a smooth Heaviside formulation as in [31]. We define

$$\mu(\phi) = \mu_1 + (\mu_g - \mu_1) H_\varepsilon(\phi), \tag{26}$$

with

$$H_\varepsilon(\phi) = \begin{cases} 0 & \text{if } \phi < -\varepsilon, \\ \frac{1}{2}\left[1 + \frac{\phi}{\varepsilon} + \frac{1}{\pi}\sin\left(\frac{\pi\phi}{\varepsilon}\right)\right] & \text{if } |\phi| \leqslant \varepsilon, \\ 1 & \text{if } \phi > \varepsilon, \end{cases} \tag{27}$$

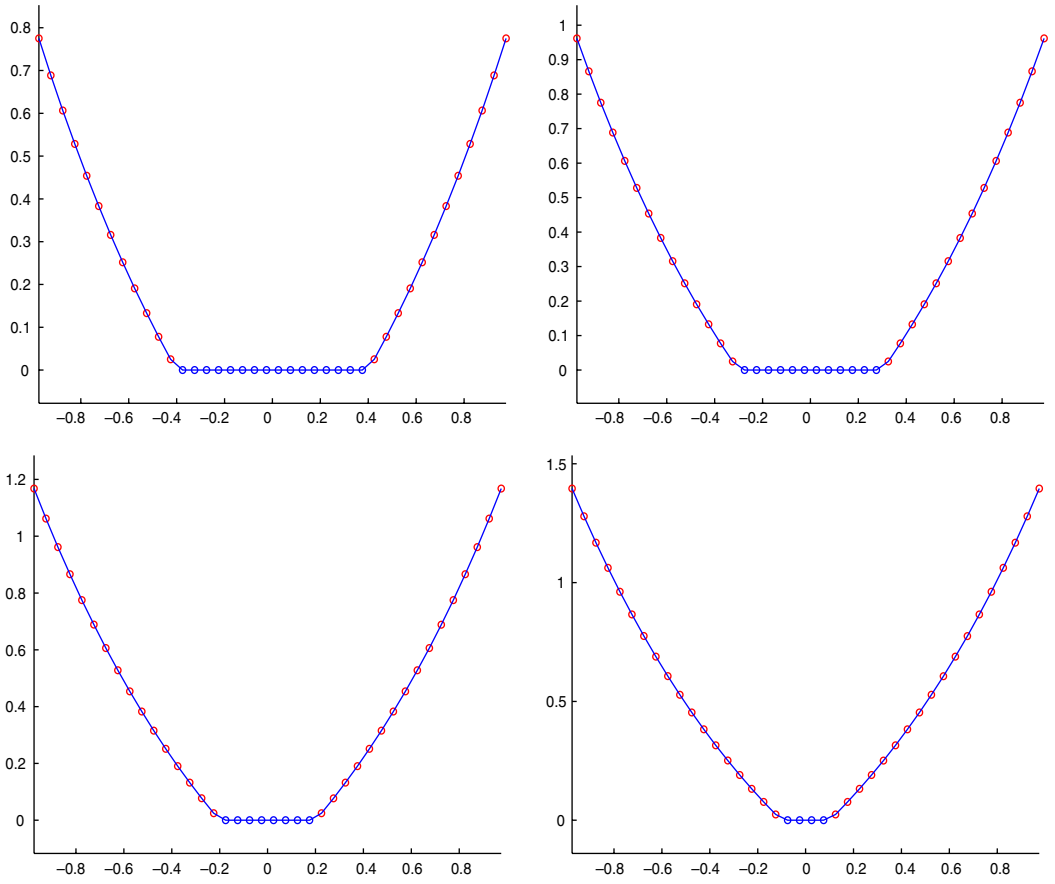

Fig. 3. One-dimensional Stefan problem with velocity constant in time. From left to right and top to bottom: temperature profile at time $t = .05$, $t = .1$, $t = .15$ and $t = .2$ computed on a grid with 40 nodes (circles) on top of the exact solution (solid line).

where ε is the interface thickness. In the numerical examples, we take $\varepsilon = 1.5\Delta x$. We emphasize that it is the only variable that is not treated in a sharp fashion.

3.4. Time evolution

We use a third-order TVD Runge–Kutta scheme (see e.g. [23] for details), which can be written as a convex combination of forward Euler steps. Adaptive time stepping is used in the examples section choosing the overall time step based on convection, viscosity, surface tension and gravity. The convective time step restriction is given by

$$\Delta t\left(\frac{|u|_{\max}}{\Delta x}+\frac{|v|_{\max}}{\Delta y}\right)\leqslant 1, \tag{28}$$

where $|u|_{\max}$ and $|v|_{\max}$ are the maximum magnitudes of the velocity in the x- and y-directions, respectively. The viscous time step restriction is given by

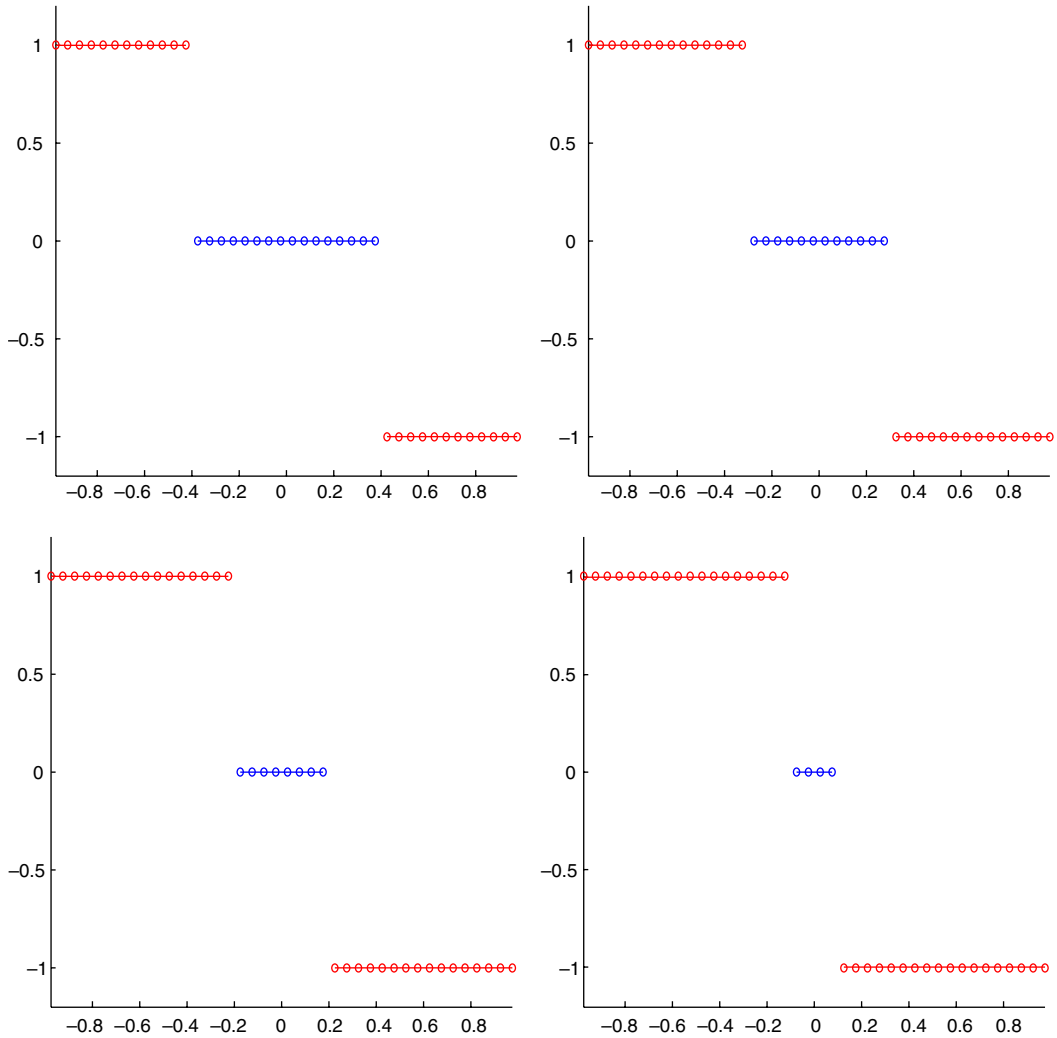

Fig. 4. One-dimensional Stefan problem with velocity constant in time. From left to right and top to bottom: velocity profile at time $t = .05$, $t = .1$, $t = .15$ and $t = .2$ computed on a grid with 40 nodes (circles) on top of the exact solution (solid line).

$$\Delta t\left(\max\left\{\frac{\mu_v}{\rho_v},\frac{\mu_l}{\rho_l}\right\}\left(\frac{2}{(\Delta x)^2}+\frac{2}{(\Delta y)^2}\right)\right)\leqslant 1. \tag{29}$$

External forces such as gravity can be included in the convection estimate given by

$$\frac{\Delta t}{2}\left((C_{\mathrm{CFL}}+V_{\mathrm{CFL}})+\sqrt{(C_{\mathrm{FL}}+V_{\mathrm{CFL}})^2+\frac{4|F_x|}{\Delta x}+\frac{4|F_y|}{\Delta y}}\right)\leqslant 1, \tag{30}$$

where C_{CFL} is the CFL number associated with the convection term and V_{CFL} is the CFL number associated with the viscosity term. $\vec{F}=(F_x,F_y)$ is the net acceleration due to forces such as gravity and surface tension [22].

4. Numerical results

In each example, the level set function ϕ is used to separate the vapor phase ($\phi\leqslant 0$) and the liquid phase ($\phi>0$).

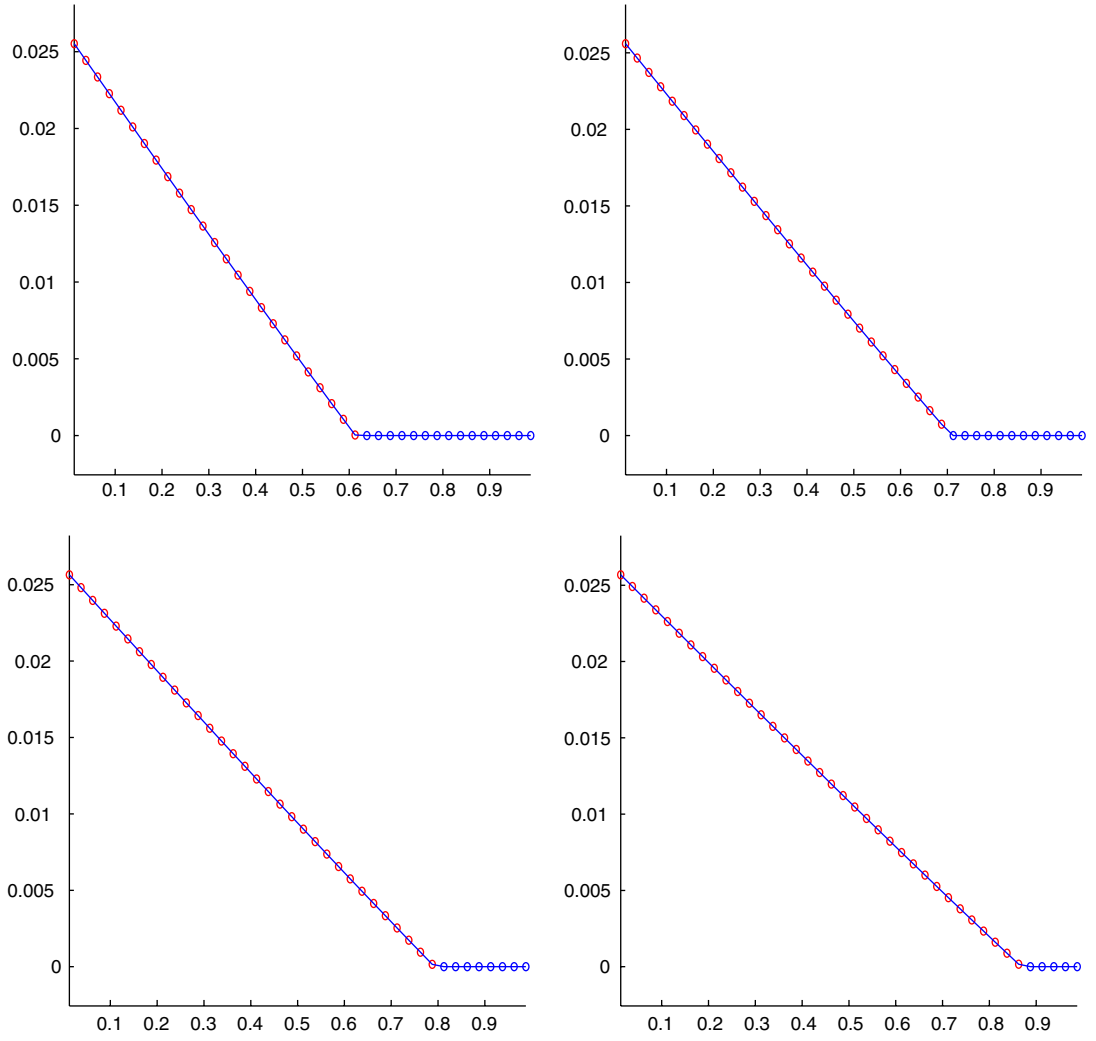

Fig. 5. One-dimensional Stefan problem with time dependent velocity. From left to right and top to bottom: temperature profile at time $t=.15$, $t=.2$, $t=.25$ and $t=.3$ computed on a grid with 40 nodes (circles) on top of the exact solution (solid line).

4.1. One-dimensional constant velocity

Consider a domain $\Omega = [-1, 1]$ with an exact solution of $T = e^{(1+v_0)t+|x|-.5} - 1$ on Ω^- and $T = 0$ on Ω^+. The liquid initially occupies the region $[-.5, .5]$, hence $\phi = .5 - |x|$. The liquid is kept at rest in Ω^-. We chose $v_0 = 1$ and set the vapor velocities to be $u = v_0$ and $u = -v_0$ on the left and right side of the interface, respectively. We take $[h_{lv}] = -1$, $k_l = k_v = 2$, $(C_p)_l = (C_p)_v = 1$, $\rho_l = 2.0$ and $\rho_v = 1.0$. Dirichlet boundary conditions for T are enforced on the domain's boundary $\partial\Omega$ using the exact solution. A Dirichlet boundary condition of $p = 0$ is also specified for the pressure on the left and right-hand side of the domain. Figs. 3 and 4 compare the exact evolution for the temperature and for the velocity, respectively with the numerical solutions computed with 40 grid points at four different times.

4.2. One-dimensional variable velocity

Consider a domain $\Omega = [0, 1]$ and a level set function $\phi = x - .5$ separating the liquid and vapor phases. The parameters we choose for the vapor phase are $k_v = 1$, $\rho_v = 0.2$ and $(C_p)_v = 5$ whereas those for the liquid

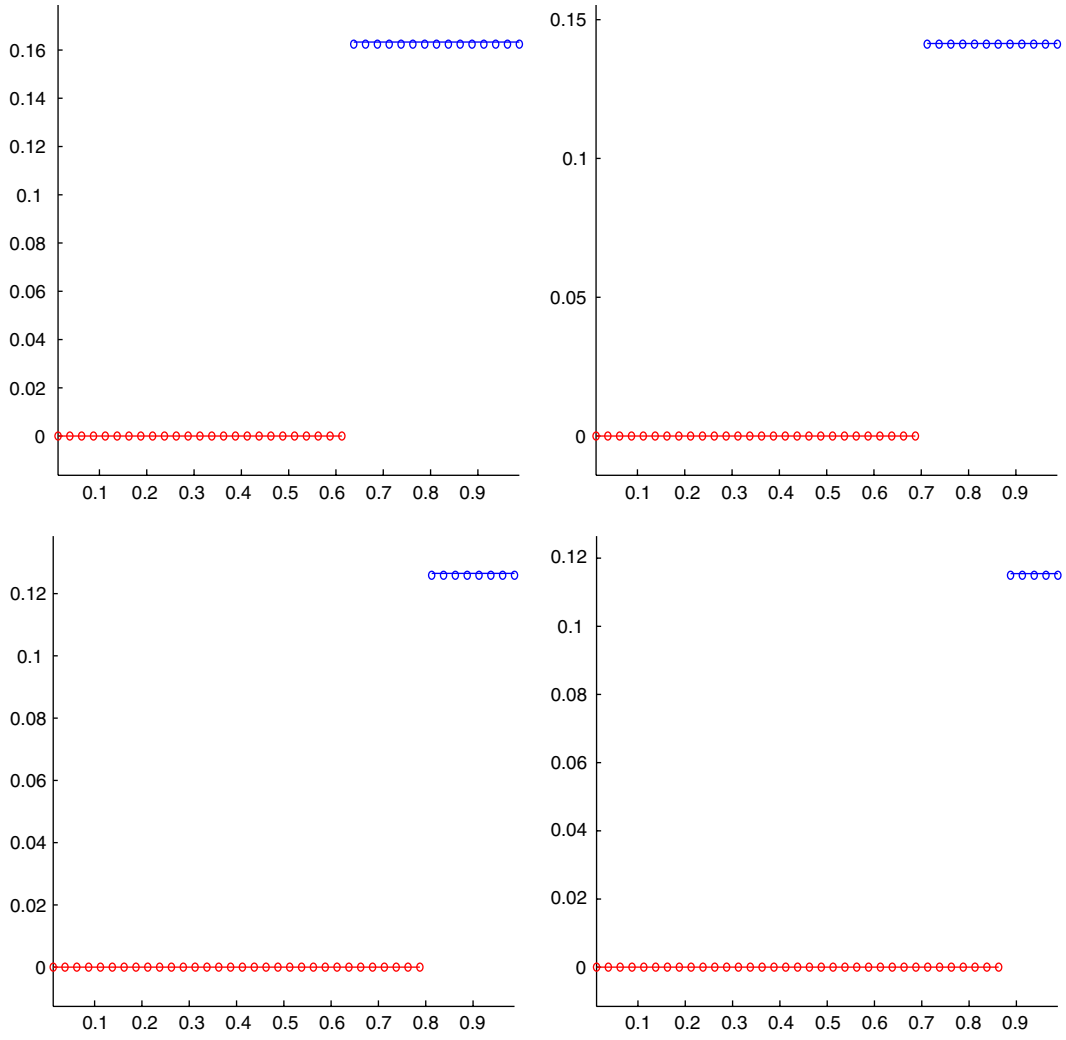

Fig. 6. One-dimensional Stefan problem with time dependent velocity. From left to right and top to bottom: velocity profile at time $t = .15$, $t = .2$, $t = .25$ and $t = .3$ computed on a grid with 40 nodes (circles) on top of the exact solution (solid line).

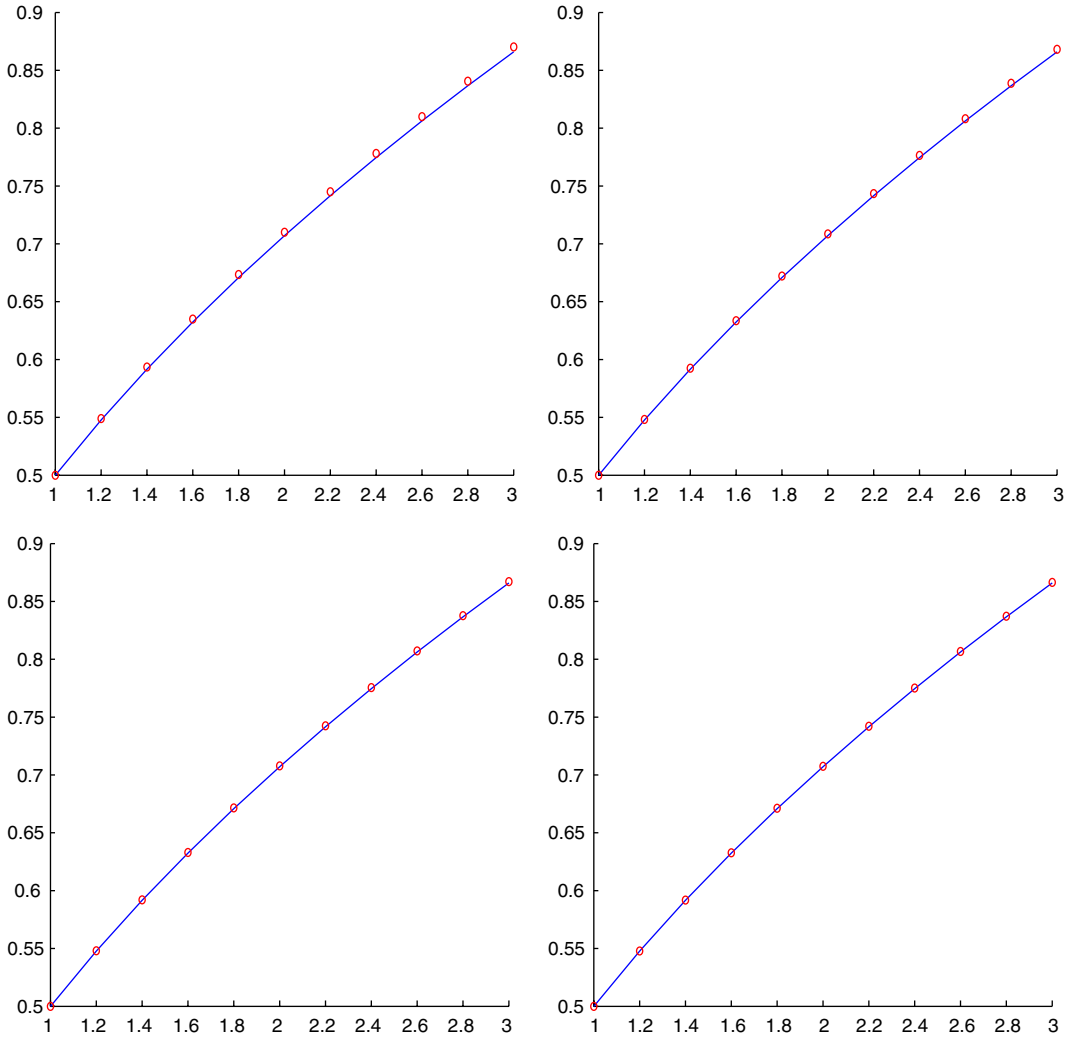

Fig. 7. Convergence under grid refinement for the one-dimensional Stefan problem with time dependent velocity. From left to right and top to bottom: evolution of the interface location computed on a grid with 20, 40, 80 and 160 nodes (circles) on top of the exact solution (solid line).

Table 1
Convergence rate for example 4.2

Number of grid nodes	Error in the interface location	Order
40	9.508×10^{-4}	–
80	4.804×10^{-4}	.98
160	2.318×10^{-4}	1.05
320	1.207×10^{-4}	.94
640	5.902×10^{-5}	1.03

phase are $k_l = 1$, $\rho_l = 1$ and $(C_p)_l = 1$. In this example, the vapor temperature increases at the wall creating a thermal profile that drives mass transfer at the interface. In this flow the vapor is motionless while the liquid is pushed away from the solid boundary, driving the interface to the right. The exact interface location is given by $\delta(t) = 2\lambda\sqrt{\alpha t}$ and the temperature for the vapor phase is given by $T(x,t) = T_{\text{wall}} + \left(\frac{T_{\text{sat}} - T_{\text{wall}}}{\text{erf}(\lambda)}\right)\text{erf}\left(\frac{x}{2\sqrt{\alpha t}}\right)$, where $\text{erf}(x) = \frac{2}{\sqrt{\pi}}\int_0^x \exp(-x^2)\,dx$ and λ is a solution to the transcendental equation $\lambda \exp(\lambda^2)\text{erf}(\lambda) =$

$\sqrt{\pi}(C_p)_v(T_{wall} - T_{sat})/h_{lv}$. Figs. 5 and 6 compare the exact evolution for the temperature and for the velocity, respectively with the numerical solutions computed with 40 grid points at four different times. Fig. 7 depicts the convergence of the numerical solution under grid refinement. Table 1 provide the accuracy analysis for the convergence of the interface location. The results are found to be accurate on a coarse grid of only 20 nodes.

4.3. Two-dimensional vaporization of a drop

In order to demonstrate the ability of our method to handle sharp jumps in the discontinuous variable, we consider the vaporization of a drop: let $\lambda = 2\pi\sqrt{3\sigma/(g(\rho_v - \rho_l))}$ and consider a domain $\Omega = [-\lambda/2, \lambda/2]^2$ with two phases separated by an interface described initially by the level set function $\phi = -\left(\sqrt{x^2 + y^2} - .5\right)$. The liquid is inside the disk. We take the surface tension $\sigma = .1$, the latent heat $h_{lv} = 10^3$ and the saturation temperature $T_{sat} = 0$. The liquid parameters are $k_l = 40$, $\rho_l = 200$, $\mu_l = .1$ and $(C_p)_l = 400$, whereas the vapor parameters are $k_v = 1$, $\rho_v = 5$, $\mu_v = .005$ and $(C_p)_v = 200$. The gravity constant is $g = 9.81$. We impose a Dirichlet boundary condition for the temperature of $T = 10$ at the domain's boundary. The vapor is allowed to exit freely from the domain. We compute the solution at $t = 6$. Fig. 8 illustrates the ability of the method to simulate flows with jumps across the interface in the velocity fields, the pressure and in the temperature gradients.

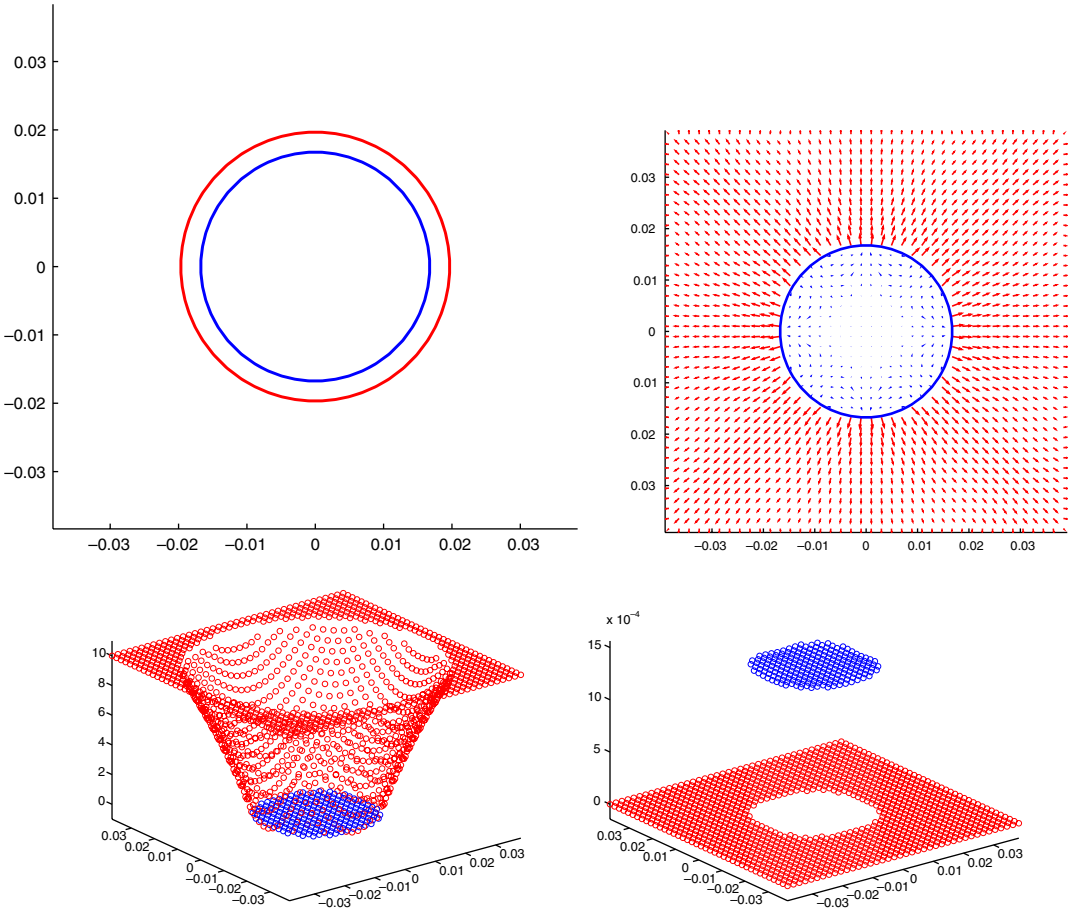

Fig. 8. Simulation of the vaporization of a drop (example 4.3). From left to right and top to bottom: interface location at $t = 0$ (red) and $t = 6$ (blue), velocity field, temperature and pressure at $t = 6$. (For interpretation of the references in colour in this figure legend, the reader is referred to the web version of this article.)

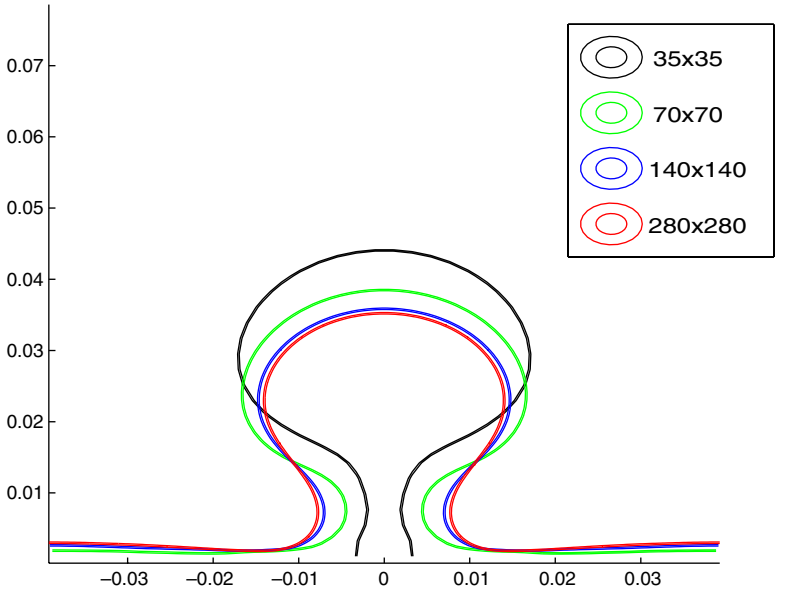

Fig. 9. Typical convergence under grid refinement for a two-dimensional boiling film simulation: interface location at time $t = 0.425$ with grid resolutions of 35×35 (black), 70×70 (green), 140×140 (blue) and 280×280 (red). (For interpretation of the references in colour in this figure legend, the reader is referred to the web version of this article.)

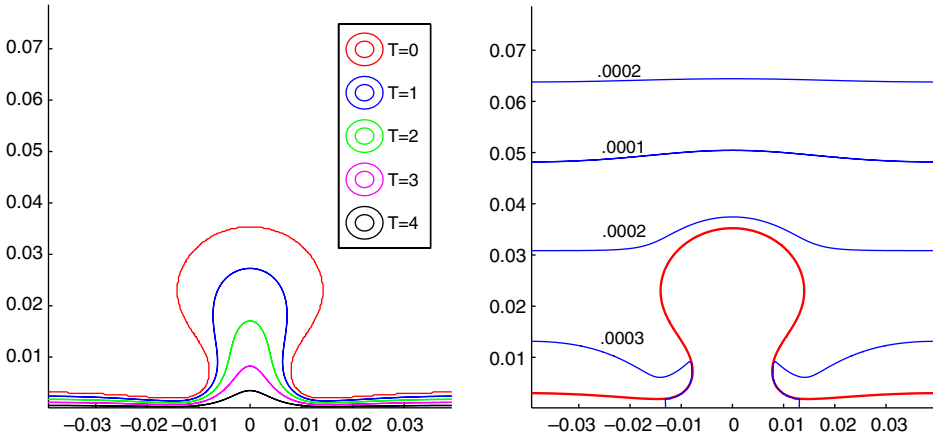

Fig. 10. Two-dimensional boiling film: temperature (left) and pressure (right) contours at time $t = 0.425$ for a grid resolution of 280×280.

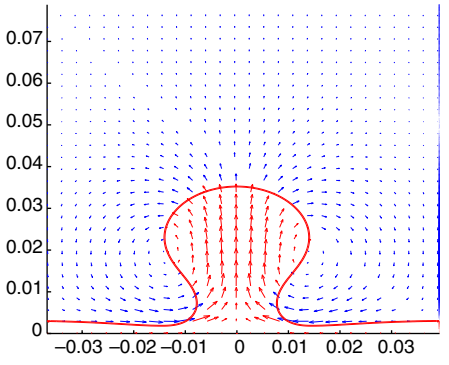

Fig. 11. Two-dimensional boiling film: velocity field at time $t = 0.425$ for a grid resolution of 280×280.

4.4. Two-dimensional film boiling

4.4.1. Convergence under grid refinement study

We now turn our attention to the simulation of thin film boiling in two spatial dimensions. In this problem, a layer of vapor is located underneath a layer of liquid and completely blankets a heated surface. A Rayleigh–Taylor instability of the liquid–vapor interface is triggered by gravity. Evaporation of the liquid as it approaches the hot wall prevents the liquid from contacting the wall and provides vapor to the rising bubbles. The liquid then falls toward the wall as the vapor rises and the cycle continues. A delicate balance is

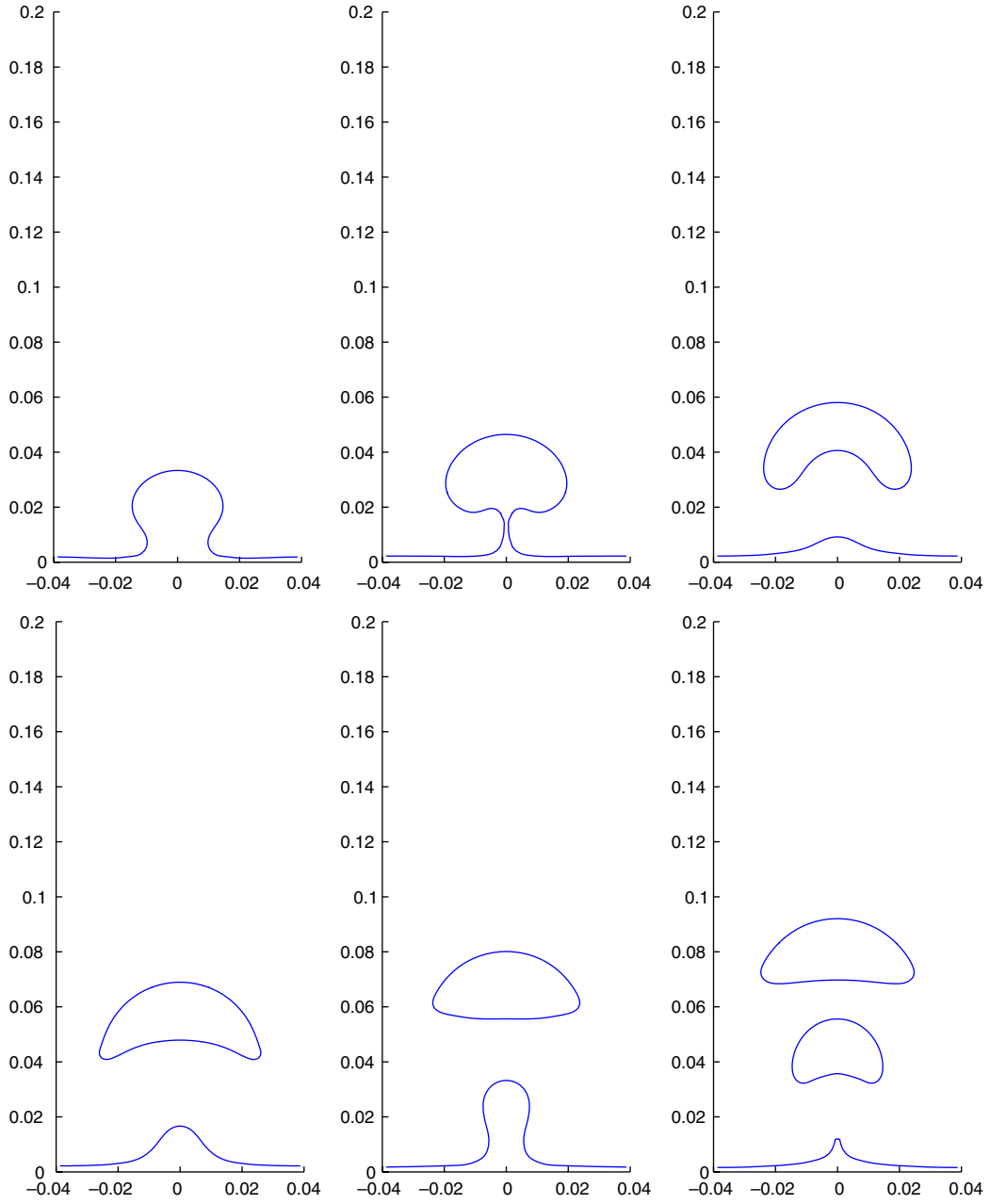

Fig. 12. Two-dimensional boiling film: the release of first two large bubbles at the early transients computed on a 64×192 grid. The time is $t = .335$ for the top left plot and is incremented by .05 for in subsequent plots.

maintained between vapor generation due to vaporization at the liquid–vapor interface and vapor removal due to the buoyancy.

We consider a two-phase fluid with surface tension $\sigma = .1$, a latent heat $h_{lv} = 10^3$, and a saturation temperature $T_{sat} = 0$. The liquid parameters are $k_l = 40$, $\rho_l = 200$, $\mu_l = .1$ and $(C_p)_l = 400$, whereas the vapor parameters are $k_v = 1$, $\rho_v = 5$, $\mu_v = .005$ and $(C_p)_v = 200$. The gravity constant is $g = 9.81$. The computations are performed in a rectangular domain that is periodic in the x-direction. The fluid is allowed to exit at the top boundary where the pressure is set to zero. The bottom boundary is considered a no-slip wall ($\vec{V} \cdot \vec{N} = 0$ and $\vec{V} \cdot \vec{T} = 0$). We initialize the liquid to be at the saturation state while the vapor temperature is set to

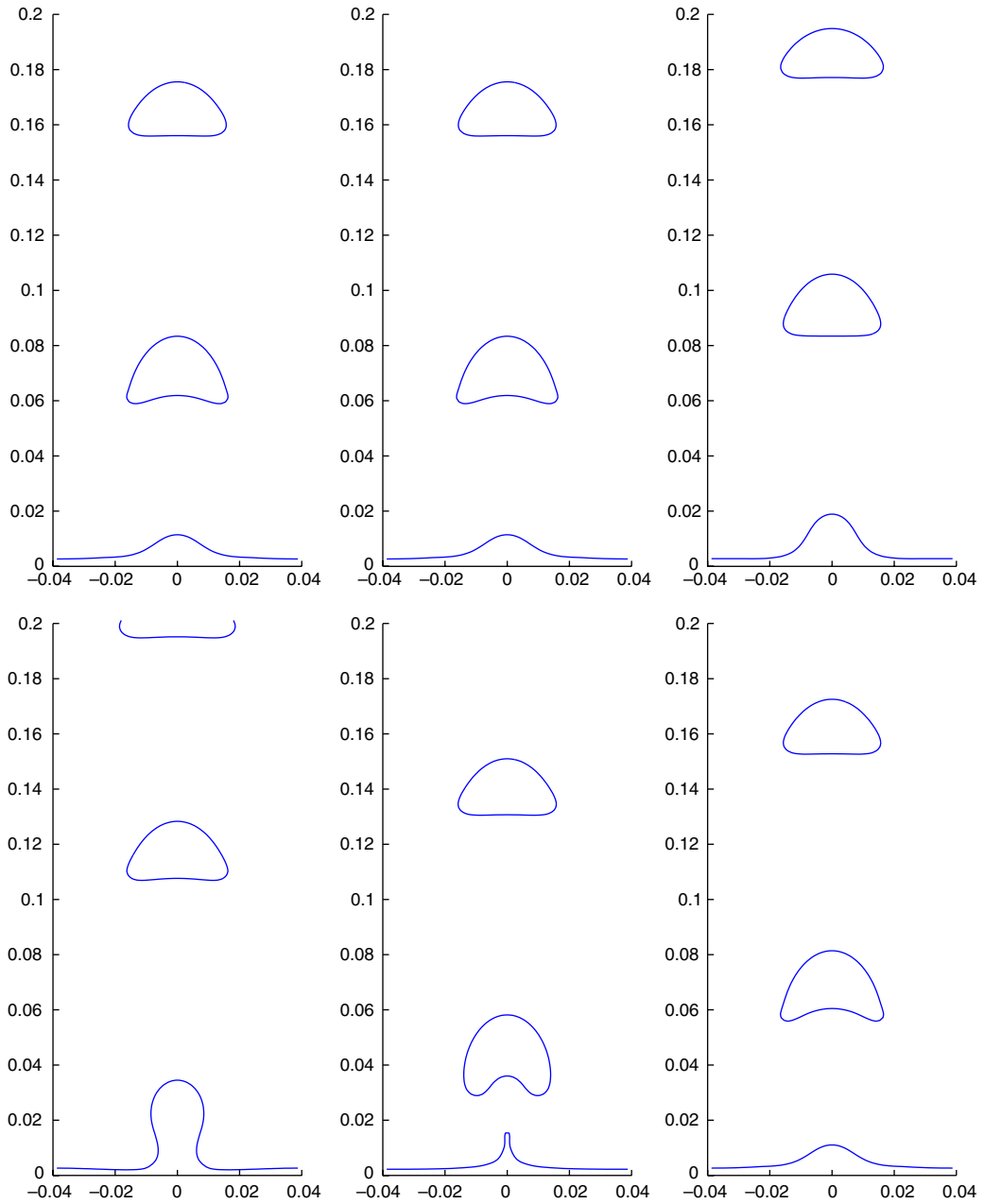

Fig. 13. Two-dimensional boiling film: quasi-steady bubble release pattern computed on a 64×192 grid. The time is $t = 1.67$ for the top left plot and is incremented by .055 in the subsequent plots.

increase linearly from the interface to the solid wall. We use a computational domain with both its width and its height equal to $\lambda = 2\pi\sqrt{3\sigma/(g(\rho_v - \rho_l))}$, the most unstable Taylor wavelength. According to Berenson [3], the distance between two consecutive vapor bubbles is equivalent to λ.

We consider four different grids with resolution 35×35, 70×70, 140×140 and 280×280. The solid wall is kept at a constant temperature of 5 K above the saturation temperature. The interface location is initialized as $y = (4 + \cos(2\pi x/\lambda))\lambda/128$. Fig. 9 depicts the convergence under grid refinement for the computed phase interface as the first bubble is about to detach from the thin film. Fig. 10 depicts the temperature and the pressure contours whereas Fig. 11 depicts the velocity field. This example demonstrates the

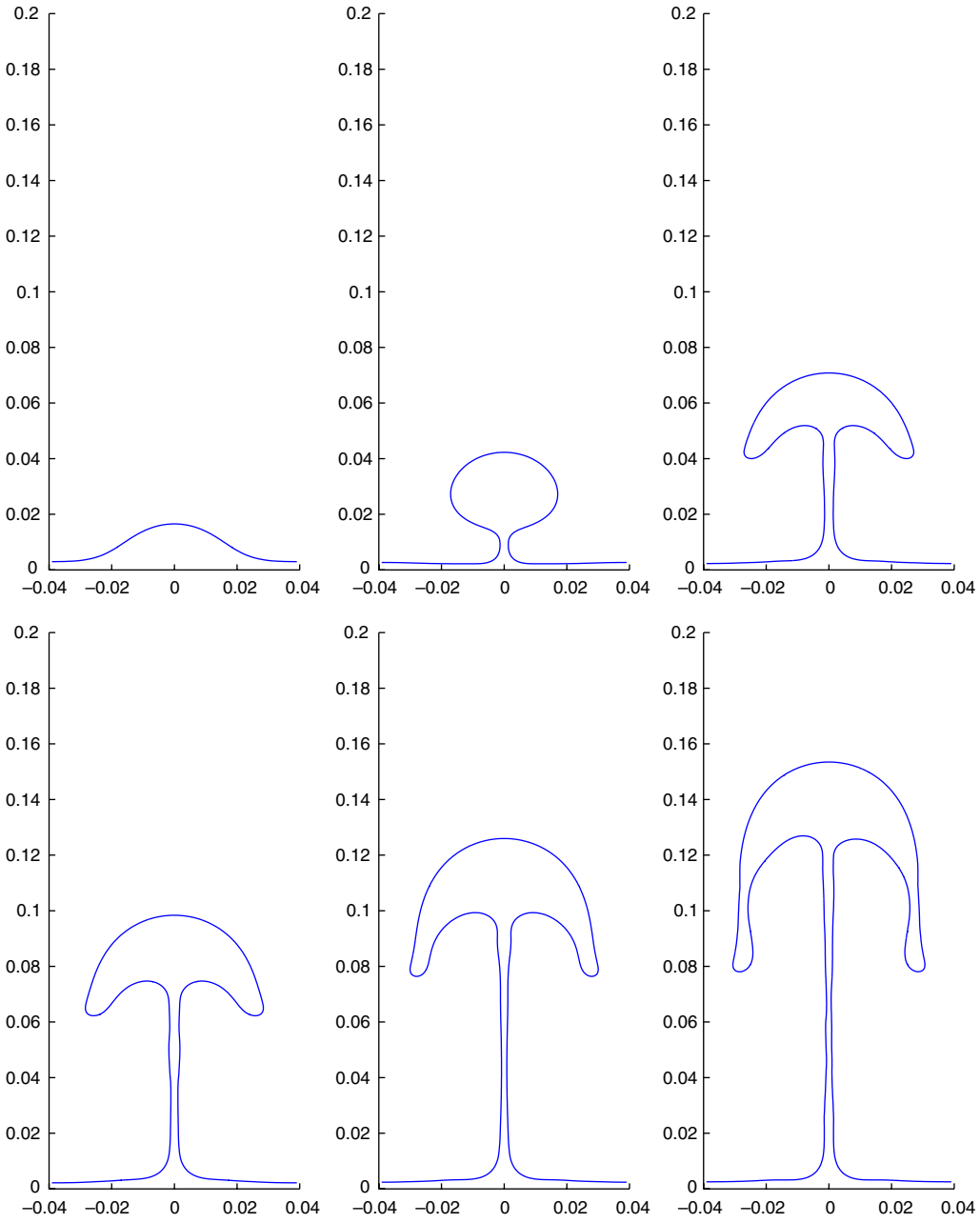

Fig. 14. Two-dimensional boiling film computed on a 140×420 grid. A mushroom shaped bubble exhibits a long stem that does not pinch off. This behavior is qualitatively correct. The time is $t = .405$ for the top left plot and is incremented by .05 in the subsequent plots.

convergence of the proposed scheme under mesh refinement and we note that convergence is achieved on fairly refined grids. Moreover, we note that the pressure contours are consistent with the shape of a two-dimensional bubble and qualitatively correct: because of the low density in the vapor phase, the pressure inside the bubble is nearly constant; on the other hand, the pressure outside is increasing from the top to the bottom of the domain due to the effects of gravity and the comparatively high density of the fluid. The bubble must then adjust the curvature of the interface to balance the pressure gradient in the liquid phase with surface tension effects.

4.4.2. Qualitative behavior

We turn our focus to the qualitative behavior of two-dimensional thin films boiling. Consider the same problem described in Section 4.4.1 with a computational domain with dimensions $\lambda \times 3\lambda$. This example has been studied by Welch and Wilson [33] using a volume-of-fluid method. We test our method on a 64×192 grid, as in [33]. Fig. 12 illustrates the early transients characterized by the release of a few large bubbles. This transient is then followed by the quasi-steady bubble release pattern, as illustrated in Fig. 13. This results are consistent with those presented in [33].

However, from the convergence study of Section 4.4.1, we conclude that a finer grid of 140×420 should be used to adequately represent the case under consideration. Fig. 14 depicts the time dependent interface shape at six different times obtained with this refined mesh. A mushroom shaped bubble develops, followed by a thin stem that supplies hot vapor to the bubble. In this case, the vapor jet persists and the bubble does not pinch off. This behavior might seem surprising, but is in fact qualitatively correct for a two-dimensional simulation: The curvature for the stem is close to zero and therefore the effects of surface tension are negligible. In fact, the same conclusion can be reached using a stability analysis as in [7]. In three spatial dimensions, one the principal curvatures would be responsible for the pinch off. Fig. 15 depicts the convergence of the flow to the thin stem under grid refinement, demonstrating that this is indeed the converged result for this simulation. Fig. 16 depicts a snapshot of the evolution at later time. Again, the stem remains but its shape is distorted by hydrodynamic instability. The qualitative results obtained on the finer grid are therefore significantly different from those obtained on a coarser grid. This demonstrates that unphysical interface breaking appear if the underlying grid is not refined enough to resolve the physical characteristic length (i.e. the stem width in our problem).

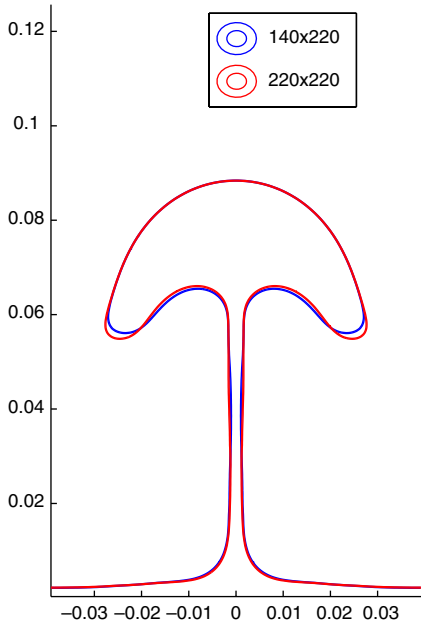

Fig. 15. Convergence under grid refinement for example 4.4.2.

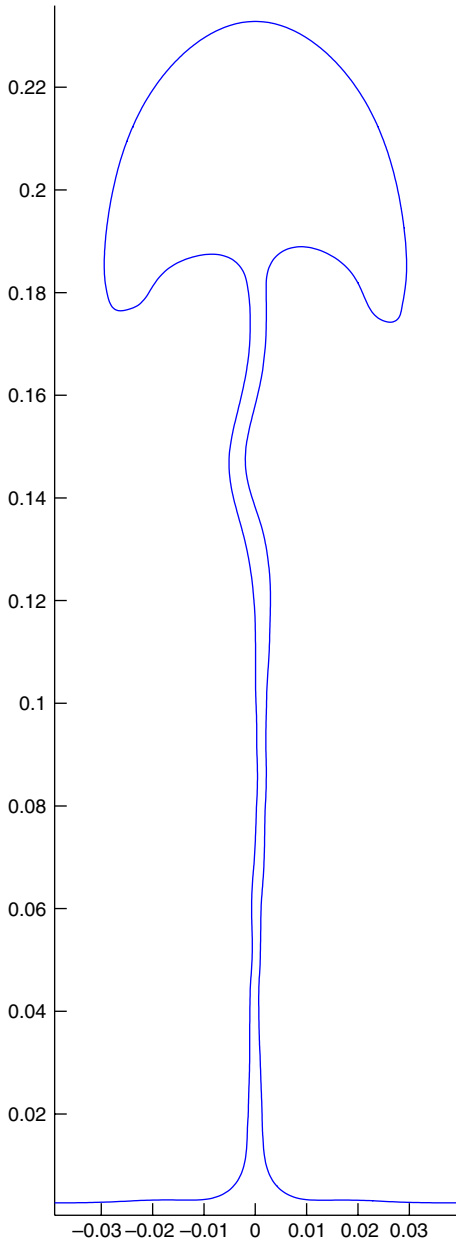

Fig. 16. Long time behavior of a two-dimensional thin film boiling: the stem does not pinch off and exhibits hydrodynamic instabilities. The time is $t = 1.3$.

5. Conclusion

We have proposed a new algorithm for multiphase flows with phase change and applied this scheme to the simulation of thin films boiling. This method takes advantage of the simplicity and robustness of the level set method to capture the interface evolution and of the ghost fluid method to impose interface's boundary conditions as introduced in [12,22]. We compared our results to exact analytical solutions and proposed a convergence study under grid refinements. We also applied this scheme to the study of thin film boiling in two spatial dimensions and obtained excellent qualitative results. In particular, we obtained results consistent with stability analysis.

Acknowledgments

Frédéric Gibou and Duc Nguyen acknowledge stimulating discussions with Ron Fedkiw while at Stanford University.

References

[1] T. Aslam, A partial differential equation approach to multidimensional extrapolation, J. Comput. Phys. 193 (2004) 349–355.
[2] P. Atkins, Physical Chemistry, fifth ed., Freeman, 1994.
[3] P.J. Berenson, Film-boiling heat transfer from a horizontal surface, J. Heat Transfer 83 (1961) 351–358.
[4] D. Brown, R. Cortez, M. Minion, Accurate projection methods for the incompressible Navier–Stokes equations, J. Comput. Phys. 168 (2001) 464–499.
[5] R. Caiden, R. Fedkiw, C. Anderson, A numerical method for two phase flow consisting of separate compressible and incompressible regions, J. Comput. Phys. 166 (2001) 1–27.
[6] A. Chorin, A numerical method for solving incompressible viscous flow problems, J. Comput. Phys. 2 (1967) 12–26.
[7] P.G. Drazin, Introduction to Hydrodynamic Stability, Cambridge University Press, New York, 2002.
[8] D. Enright, R. Fedkiw, J. Ferziger, I. Mitchell, A hybrid particle level set method for improved interface capturing, J. Comput. Phys. 183 (2002) 83–116.
[9] R. Fedkiw, The ghost fluid method for discontinuities and interfaces, in: E.F. Toro (Ed.), Godunov Methods, Kluwer, New York, 2001.
[10] R. Fedkiw, T. Aslam, B. Merriman, S. Osher, A non-oscillatory Eulerian approach to interfaces in multimaterial flows (the ghost fluid method), J. Comput. Phys. 152 (1999) 457–492.
[11] F. Gibou, R. Fedkiw, A fourth order accurate discretization for the Laplace and heat equations on arbitrary domains, with applications to the Stefan problem, J. Comput. Phys. 202 (2005) 577–601.
[12] F. Gibou, R. Fedkiw, L.-T. Cheng, M. Kang, A second-order-accurate symmetric discretization of the Poisson equation on irregular domains, J. Comput. Phys. 176 (2002) 205–227.
[13] G. Golub, C. Loan, Matrix Computations, The John Hopkins University Press, 1989.
[14] R. Guy, A. Fogelson, Stability of approximate projection methods on cell-centered grids, J. Comput. Phys. 203 (2005) 517–538.
[15] F. Harlow, J. Welch, Numerical calculation of time-dependent viscous incompressible flow of fluid with free surface, Phys. Fluids 8 (1965) 2182–2189.
[16] M. Ishii, Thermo-Fluid Dynamic Theory of Two-Phase Flow, Eyrolles, Paris, 1975.
[17] G.-S. Jiang, D. Peng, Weighted ENO schemes for Hamilton–Jacobi equations, SIAM J. Sci. Comput. 21 (2000) 2126–2143.
[18] D. Juric, G. Tryggvason, Computations of boiling flows, Int. J. Multiphase Flow. 24 (1998) 387–410.
[19] M. Kang, R. Fedkiw, X.-D. Liu, A boundary condition capturing method for multiphase incompressible flow, J. Sci. Comput. 15 (2000) 323–360.
[20] X.-D. Liu, S. Osher, T. Chan, Weighted essentially non-oscillatory schemes, J. Comput. Phys. 126 (1996) 202–212.
[21] X.D. Liu, R. Fedkiw, M. Kang, A boundary condition capturing method for Poisson's equation on irregular domains, J. Comput. Phys. 154 (2000) 151.
[22] D. Nguyen, R. Fedkiw, M. Kang, A boundary condition capturing method for incompressible flame discontinuities, J. Comput. Phys. 172 (2001) 71–98.
[23] S. Osher, R. Fedkiw, Level Set Methods and Dynamic Implicit Surfaces, Springer-Verlag, New York, NY, 2002.
[24] S. Osher, J. Sethian, Fronts propagating with curvature-dependent speed: Algorithms based on Hamilton–Jacobi formulations, J. Comput. Phys. 79 (1988) 12–49.
[25] R. Peyret, T. Taylor, Computational Methods for Fluid Flow, Springer-Verlag, New York, 1983.
[26] Y. Saad, Iterative Methods for Sparse Linear Systems, PWS Publishing, New York, NY, 1996.
[27] J.A. Sethian, Level Set Methods and Fast Marching Methods, Cambridge University Press, Cambridge, 1999.
[28] C.-W. Shu, S. Osher, Efficient implementation of essentially non-oscillatory shock capturing schemes II (two), J. Comput. Phys. 83 (1989) 32–78.
[29] G. Son, V. Dhir, Numerical simulation of saturated film boiling on a horizontal surface, J. Heat Transfer 119 (1997) 525.
[30] G. Son, V. Dhir, Numerical simulation of film boiling near critical pressures with a level set method, J. Heat Transfer 120 (1998) 183.
[31] M. Sussman, P. Smereka, S. Osher, A level set approach for computing solutions to incompressible two-phase flow, J. Comput. Phys. 114 (1994) 146–159.
[32] S. Welch, Local simulation of two-phase flows including interface tracking with mass transfer, J. Comput. Phys. 121 (1995) 142.
[33] S. Welch, J. Wilson, A volume of fluid based method for fluid flows with phase change, J. Comput. Phys. 160 (2000) 662.
[34] G. Tomar, G. Biswas, A. Sharma, A. Agrawal, Numerical simulation of bubble growth in film boiling using a coupled level-set and volume-of-fluid method, Phys. Fluid 14 (2005) 112103.